Pergamon

Int. J. Mach. Tools Manufact. Vol. 35, No. 5, pp. 689–699, 1995

0890–6955/95$9.50 + .00

DETERMINATION OF THE RADIAL WIDTH OF CUT AND CUTTING MODES IN MILLING

S. HINDUJA,† Y. S. MA† and G. BARROW†

(*Received* 3 *June* 1994)

Abstract—This paper describes a method to calculate the variation in the radial width of cut which occurs when the centre of a milling cutter follows the toolpath segments generated by a postprocessor. This variation is approximated by a stepped curve, thus enabling the toolpath segment to be divided into subsections, the radial width remaining constant over each subsection. The method also enables the cutting modes to be determined. The variation in the width of cut is obtained by performing a 2-D Boolean union between the area swept by the cutter when traversing the current segment and the area already machined. As an example, the actual widths of cut are calculated for the toolpaths for machining a pocket. The example clearly demonstrates that the actual widths of cut vary over a wide range and are very different from the value used to calculate the toolpaths. In fact, for the example considered, slotting occurs over 40% of the distance travelled, and only 10% of the actual widths of cut are approximately equal to the original value used for toolpath generation.

1. INTRODUCTION

IN RECENT years there have become available several computer-aided process planning systems for turned and milled components. An important function of these systems is the determination of the optimum cutting conditions. This requires an exact knowledge of the cutting geometry which, in the case of milling, comprises the radial width of cut, the mode of milling and the axial depth of cut. If these parameters are known, the cutting parameters (feedrate and velocity) can be optimized subject to several constraints.

In $2\frac{1}{2}$-D milling, since the axial depth of cut is constant for a given pass, the radial width of cut becomes the major parameter required to predict the cutting force.

The post-processing modules of the process planning systems generate, as their output, a series of straight-line and circular arc segments which the centre of the cutter follows. In the case of milling, these centre line (CL) toolpath segments form a zig, zig-zag or spiral-shaped pattern. In the case of pocket milling, an outward spiral-shaped tool path is often preferred as it minimizes the amount of slotting. With these paths, the radial width of cut does not remain constant as the cutter travels from one end of the segment to the other. This is true even if the neighbouring segments are parallel to the current segment. Variations in the radial width of cut cause the resulting cutting force to fluctuate and in critical regions, such as corners, Kline *et al.* [1] have reported that the force can increase by a factor of 10. Such critical regions may cause chatter or even tool breakage. Wang [2] suggested that the feedrate be changed according to the "in-process geometry" so that the cutting force is under control. In this paper the variation in the radial width of cut is calculated and then approximated by a stepped curve, thus enabling the toolpath segment to be subdivided into sections, the radial width, and thus the feedrate, remaining constant over each subsection. There is no reported work on the determination of the radial width of cut. Some 3-D systems [2–5] can simulate the cutting geometries for each cutter motion, but the computing time becomes prohibitive for the optimization process. Other 3-D simulation systems [6–8] have been used for graphical collision checking but not for calculating the cutting geometry.

†Manufacturing Division, Department of Mechanical Engineering, UMIST, Manchester, U.K.

2. TERMINOLOGY

To explain the definitions given below, assume the cutter centre moves from the start vertex, P_1, to P_2, the end vertex of the first segment, and then from P_2 to P_3, etc. [see Fig. 1(a)].

(i) Swept Area: the area enclosed by the envelope curve generated by the cutter as it travels from the start vertex to the end vertex of the given segment. The swept area of the cutter travelling along a straight line is shown in Fig. 2. If the cutter moves from P_1 to P_2, then $P_{01}P_{02}P_{m2}P_{i2}P_{i1}P_{m1}P_{01}$ forms the boundary of the swept area. The boundary curve can be subdivided into the following:

(a) Outer Bound (OB): the offset of the toolpath segment by the cutter radius in the direction given by $-S \times P_1P_2$, where S is the normal to the boundary profile.

(b) Inner Bound (IB): the offset of the toolpath segment by the cutter radius in the direction given by $S \times P_1P_2$.

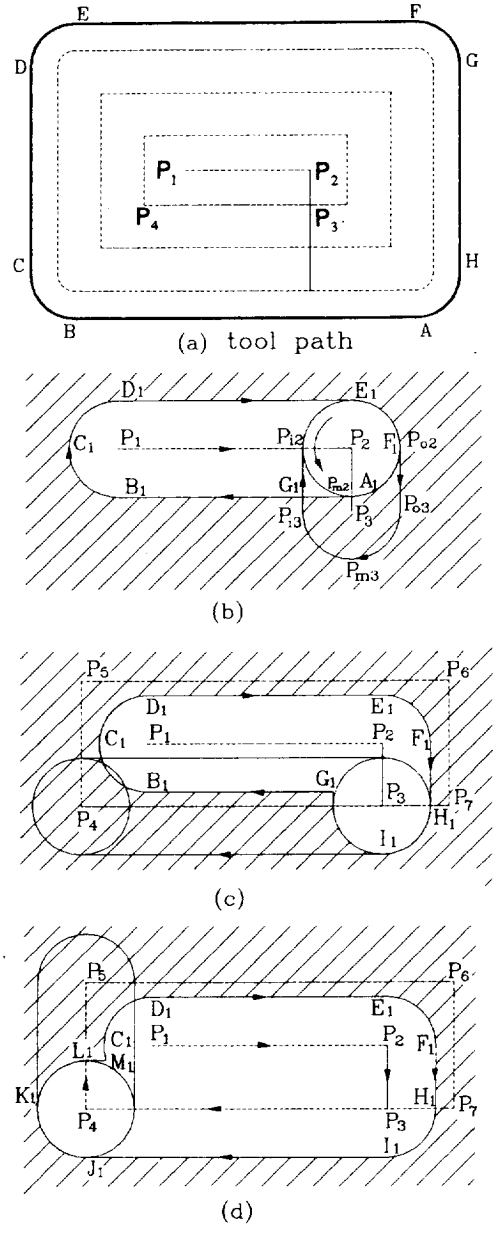

FIG. 1. Derivation of the machined graph.

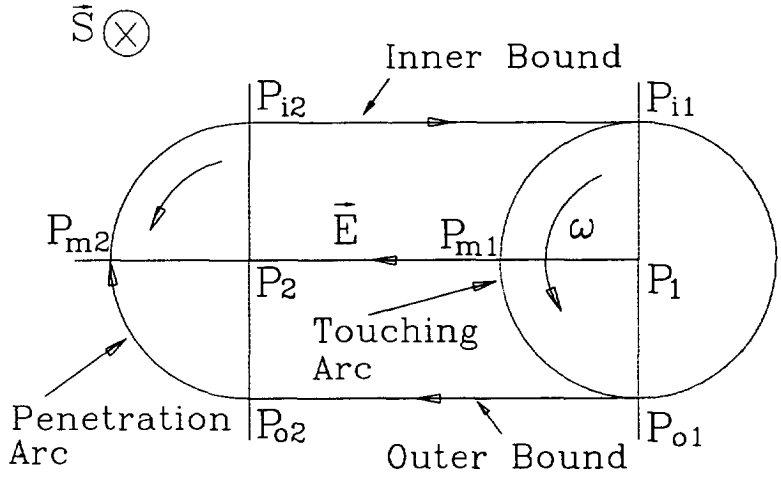

FIG. 2. Cutter swept area.

(c) Touching Arc (TA): the blending arc between the outer and inner bounds when the cutter is positioned at the start vertex of the segment.

(d) Penetration Arc (PA): the blending arc between the outer and inner bounds when the cutter is positioned at the end vertex of the segment.

In Fig. 2, $P_{01}P_{02}$, $P_{i2}P_{i1}$, $P_{i1}P_{m1}P_{01}$ and $P_{02}P_{m2}P_{i2}$ are referred to as the outer bound, inner bound, touching arc and penetration arc, respectively. Points P_{01} and P_{i1} are referred to as the start and end points of the swept area, respectively, because the outer bound, penetration arc and inner bound either start from P_{01} or end at P_{i1}.

(ii) Machined Graph: the envelope of the total area swept by the cutter in its prevous movements. Since the boundary of the machined area is represented as a graph in the data structure of a solid modeller, it is referred to as a machined graph. The machined graph develops as the cutter traverses each CL segment.

(iii) Cutting Geometry Diagram: a 2-D Boolean union between the machined graph and the current swept area.

A simple example is shown in Fig. 1(a). The pocket boundary is given by ABCDEFGHA and the toolpath segments by P_1P_2, P_2P_3, P_3P_4, etc. The swept area, defined by the boundary $A_1B_1C_1D_1E_1F_1A_1$ [Fig. 1(b)], becomes the machined graph for the next segment. When the cutter moves from P_2 to P_3, the material enclosed by the swept area $P_{02}P_{03}P_{m3}P_{i3}P_{i2}$ $P_{m2}P_{02}$ is machined. For this segment, the cutting geometry diagram is given by $G_1B_1C_1D_1E_1F_1P_{03}$ $P_{m3}P_{i3}G_1$. The current swept area intersects with the machined graph at points G_1 and F_1. After segment P_2P_3 has been traversed, the machined graph is updated to $H_1I_1G_1B_1C_1D_1E_1F_1H_1$, shown in Fig. 1(c). After P_3P_4 has been traversed, the new machined graph becomes $J_1K_1L_1M_1C_1D_1E_1F_1H_1$ I_1J_1 [Fig. 2(d)]. In this manner, the machined graph is derived in stages.

3. DETERMINATION OF THE CUTTING GEOMETRY DIAGRAM

The cutting geometry diagram is obtained by performing a Boolean union between the swept area and machined graph. For any 2-D Boolean operation [9], the intersection points between the boundaries enclosing the two areas must be first determined.

It can be appreciated that the touching arc has no intersection with the machined graph because it is either partially coincident with a segment of the machined graph or enclosed completely by the machined graph. Therefore, the intersection points must lie on the outer and inner bounds, and the penetration arc. The total number of intersection points is always even. For example, Fig. 3 shows a machined graph which intersects the boundary of the current swept area at four positions. After the intersection points are obtained, the machined graph is traversed, starting from a point on its boundary. This point should not lie on the boundary of the swept area. At the first

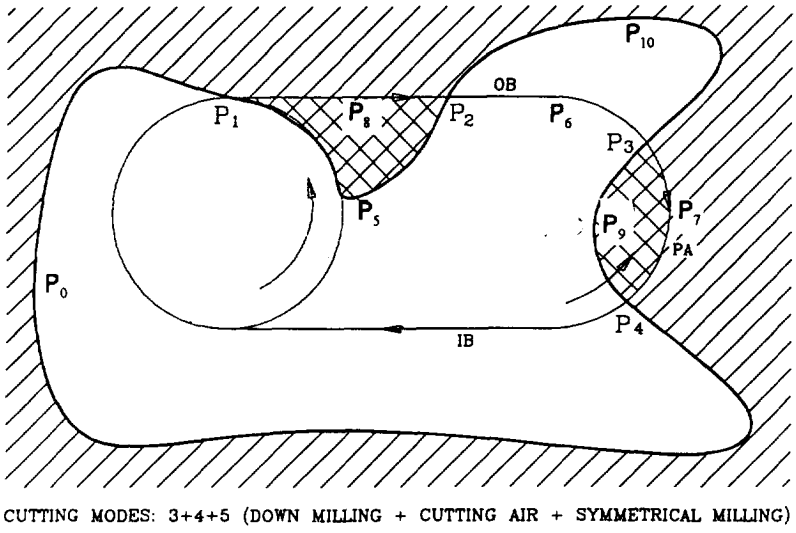

FIG. 3. Updating the machined graph.

intersection point, the traversing is switched from the machined graph to the boundary of the swept area. In this manner, the traversing is continued until the start point is reached. This results in some segments of the machined graph being discarded and replaced by segments from the swept area boundary. Segments of the machined graph that are enclosed by the current swept area are discarded.

Figure 3 shows an example where the traversing starts from point P_0. Upon reaching P_1, the traversing is switched to the outer bound (OB, see Fig. 3) of the swept area boundary. At the next intersection point P_2, the traversing is switched back to the machined graph. Meanwhile segments $P_1P_5P_2$ on the machined graph are replaced by segments $P_1P_8P_2$ of the swept area boundary. Travelling from P_2 to P_3 via P_{10} on the machined graph means that segments $P_2P_6P_3$ on the outer bound and penetration arc are ignored. On reaching P_3, travel is switched to the swept area boundary and at P_4, travel is continued on the machined graph. This alternate switching from the machined graph to the swept area boundary results in the cutting geometry diagram which, in this example, is given by $P_0P_1P_8P_2P_{10}\ P_3P_7P_4P_0$.

4. CUTTING MODES

Traditionally, the cutting modes considered in milling are up-milling, down-milling and slotting. However, according to Lau [10], this classification is far too rigid and he suggests the following cutting modes (Fig. 4): down-milling, up-milling, slotting, symmetrical milling, pro-down-milling, pro-up-milling and combined milling. This classification is based on the cutter force direction, entry and exit angles and effective chip thickness. Obviously, these parameters are determined by where the cutter enters and leaves the work material and therefore the type of cutting mode present can be determined by examining the positions of the cutter entry and exit points. For this purpose, the semi-circle swept by the cutter is partitioned into four zones (Fig. 5). The different cutting modes are also shown as horizontal bars, the length of which represents the cutter tooth swept ranges. The traditional definitions of the cutting mode are quite rigid—in slotting, both the cutter tooth entry and exit angles must be 0°. However, in order to cater for the additional cutting modes suggested, more flexible definitions are required (see Table 1).

The most suitable value for α is a matter for discussion. A value of 30° has been used by the authors.

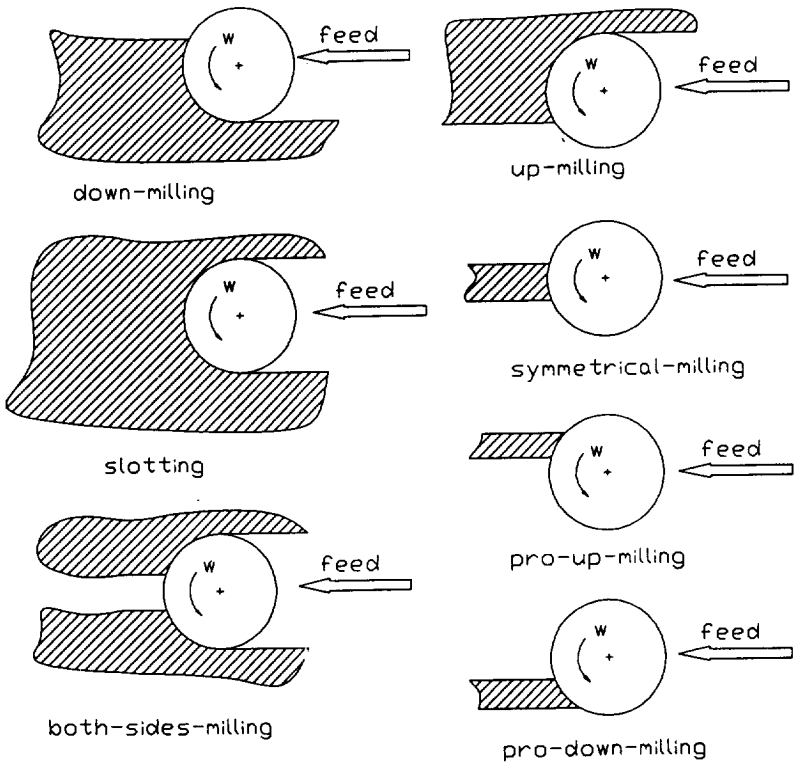

FIG. 4. Different cutting modes.

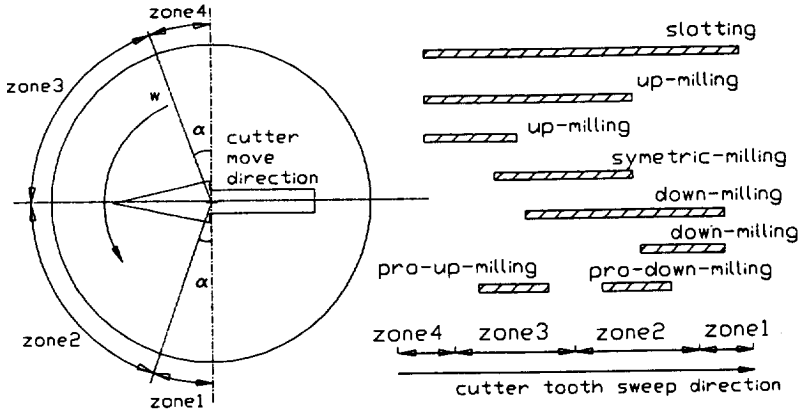

FIG. 5. Definition of cutting modes.

TABLE 1. DEFINITION OF CUTTING MODES

Entry point	Exit point	Cutting mode
Zone 4	Zone 1	Slotting
Zone 4	Zone, 4, zone 3 or zone 2	Up-milling
Zone 3, zone 2 or zone 1	Zone 1	Down-milling
Zone 3	Zone 2	Symmetrical milling
Zone 3	Zone 3	Pro-up-milling
Zone 2	Zone 2	Pro-down-milling

TABLE 2. CUTTER EXIT AND ENTRY POSITIONS FOR DIFFERENT CUTTING MODES

Entry point on	Exit point on	Cutting mode
Outer bound	Outer bound	Down-milling
Outer bound	Penetration arc	Down-milling
Outer bound	Inner bound	Down-/up-milling or slotting
Penetration arc	Penetration arc	Pro-down-/up- or symmetrical milling
Penetration arc	Inner bound	Up-milling
Inner bound	Inner bound	Up-milling

5. DETERMINATION OF THE CUTTING MODE

Assuming that there is only one pair of intersection points, i.e. one lump of stock area, the positions of the entry and exit points on the boundary of the current swept area determine the cutting mode. The complete relationship between the positions and the cutting mode is summarized in Table 2.

If there are two or more disjoint lumps of stock areas, each lump is analysed individually. It is also possible that two different modes of milling, i.e. combined milling, may occur.

In Fig. 1(b), when the cutter moves from P_1 to P_2, the cutting mode is obviously slotting. From P_2 to P_3, the cutting mode is initially down-milling and the radial width of cut increases gradually until the cutter periphery touches G_1 when the cutting mode changes to slotting.

6. ACTUAL RADIAL WIDTH OF CUT

Although the term radial width of cut is commonly used in practice, there is no strict definition for it. A possible definition to cover all the milling modes is as follows:

"The radial width of cut is the distance between the entry and exit points, the distance being measured in a direction perpendicular to the feed vector. If there is more than one pair of entry and exit vertices, then it is the cumulative sum of the distances between the entry and exit points."

In Fig. 6, three cutting modes are shown with the cutter centre traversing a straight-line segment from P_1 to Q. In Fig. 6(a), the cutting mode is down-milling and the hatched area represents the material to be removed. A, B and C are three points on the machined graph that are enclosed in the current swept area. When the cutter reaches points A, B and C, the cutter centre is at positions P_1, P_2 and P_3, respectively. The radial width of cut in the down-milling mode is the distance of the entry point on the curve ABC from the outer bound of the current swept area or its extension. Note that this width of cut changes continuously as the cutter centre moves along the CL

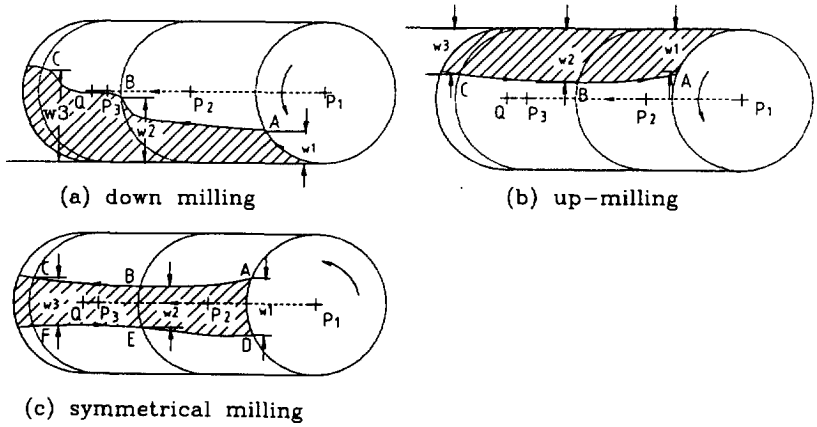

FIG. 6. Radial width of cut for different cutting modes.

segment. In Fig. 6(a), when the cutter reaches position P_1, the entry point is A, and its distance (w_1) from the outer bound defines the width of cut. Similarly, w_2 and w_3 are the widths of cut when the cutter is at positions P_2 and P_3, respectively.

In Fig. 6(b), the cutting mode is up-milling. The width of cut in this cutting mode is the distance from the exit point to the inner bound or its extension. The widths of cut at A, B and C are labelled as w_1, w_2 and w_3, respectively.

In Fig. 6(c), the cutting mode is symmetrical milling. The width of cut is given by the distance between lines which are drawn through the entry and exit positions and are parallel to the given CL segment. In this particular case, it is the distance between the curves ABC and DEF. The widths at P_1, P_2 and P_3 are labelled as w_1, w_2 and w_3, respectively.

6.1. *Approximating the varying width of cut*

As shown in Fig. 6, the radial width of cut varies continuously over the segment, and this makes it computationally expensive to calculate the radial width of cut at each and every point along the toolpath segment. The variation in the radial width of cut can be approximated by a stepped profile. This has the advantage that the width of cut can be assumed to be constant over each section of the segment which, in turn, will enable the feedrate to be tuned to its optimum value over each section. The stock profile in Fig. 7(a) is represented by a stepped curve in Fig. 7(b). Note that the height of the step indicated in the figure represents the maximum width of cut occurring over that section.

Although the stock is represented as a stepped profile, there are transient situations which need special attention. These correspond to the vertical segment on the stepped profile. As before, a constant width of cut must be assumed over this vertical segment, with a value equal to the maximum width of cut occurring over the vertical section. Figure 7(c) shows a stepped profile, part of which is labelled as UV. The cutter reaches V first, after which the width of cut increases gradually, reaching its maximum value at U. The corresponding cutter centre positions are at X and Y, respectively. The width of cut when the cutter touches U is used for the subsection XY of the segment. In Fig. 7(d), when the cutter moves from X to Y, it reaches V first again, but the actual width of cut keeps decreasing as the cutter moves towards U. For the subsection

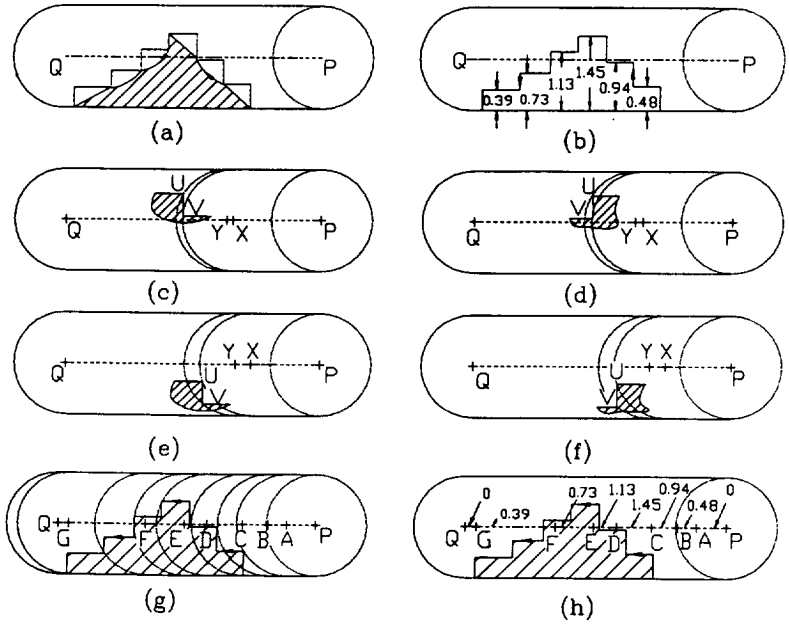

FIG. 7. Stepped approximation for the radial width of cut.

XY in Fig. 7(e), the width of cut occurring at Y is used while in Fig. 7(f), the radial width of cut occurring at X is used for the subsection. Figure 7(g) shows the original toolpath segment PQ is split into subsections PA, AB, BC, etc. where A, B, C are the cutter centre positions. Figure 7(h) shows the corresponding widths of cut for each subsection of the segment. Note that the cutter is cutting fresh air over the first and last subsection.

In the above example, the cutting mode is down-millling and a similar technique can be used for up-milling. For symmetrical milling, however, the procedure has to be slightly modified since neither the entry nor the exit points lie on the boundary of the swept area. Instead they lie on the stock profile which is usually U-shaped. The stock profile is first approximated by a stepped curve and then the distance of each step from one of the bounds is determined [Fig. 8(a) and (b)]. Then the toolpath segment PQ is divided into two independent sets of subsections, one for the upper part and the other for the lower [Fig. 8(c)]. These two sets are then merged together, making it necessary to subdivide PQ into more subsections, thus ensuring that the radial width of cut remains constant over each subsection. The resulting subdivision and the values associated with each subsection are indicated in Fig. 8(d).

This method can also be used for pro-down-milling and pro-up-milling. For slotting, the width of cut can be assumed to be equal to the cutter diameter.

It is possible that the cutting geometry diagram is such that combined cutting modes occur. Figure 9(a) shows a situation where the cutting mode is first up-milling and then down-milling. The calculation procedure for such situations is divided into sub-procedures, each procedure dealing with a specific cutting mode. The final effective width of cut can then be calculated by merging the two independent sets of stepped profiles and radial widths of cut. The lower stock area in Fig. 9 is represented by the stepped profile in Fig. 9(b), the step heights being 0, 0.27, 0.63 and 0.44, and the tool segment PQ being split at A, B and C. Similarly, the upper stock is represented by the stepped curve in Fig. 9(c), the step heights being 0, 0.31, 0.48, 0.19 and 0, and the toolpath segment being split at D, E, F and G. The merged radial widths of cut and the final subdivision of the toolpath segment are shown in Fig. 9(d).

7. EXAMPLE

Figure 10(a) shows a pocket, the toolpath segments for which have been generated assuming a cutter diameter of 14 mm and a radial width of cut of 9.8 mm. In all, the postprocessor generated 100 segments and these are shown in Fig. 10(b). Using the technique described in this paper, they were further subdivided resulting in 130

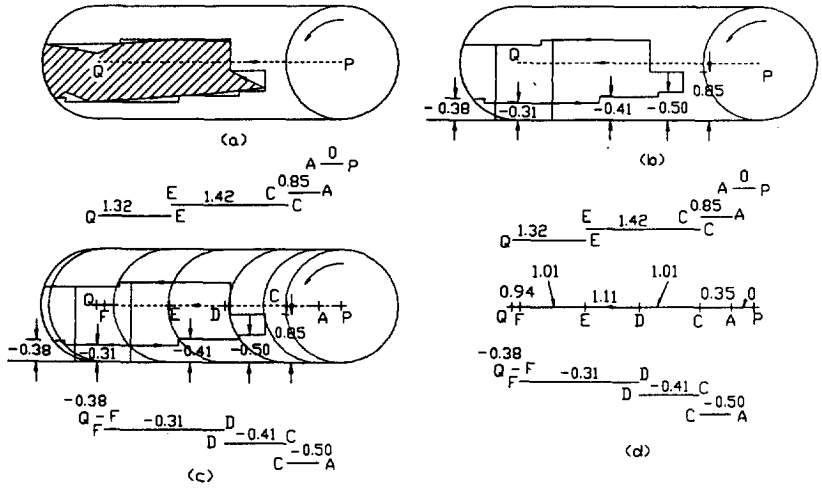

FIG. 8. Radial width of cut in symmetrical milling.

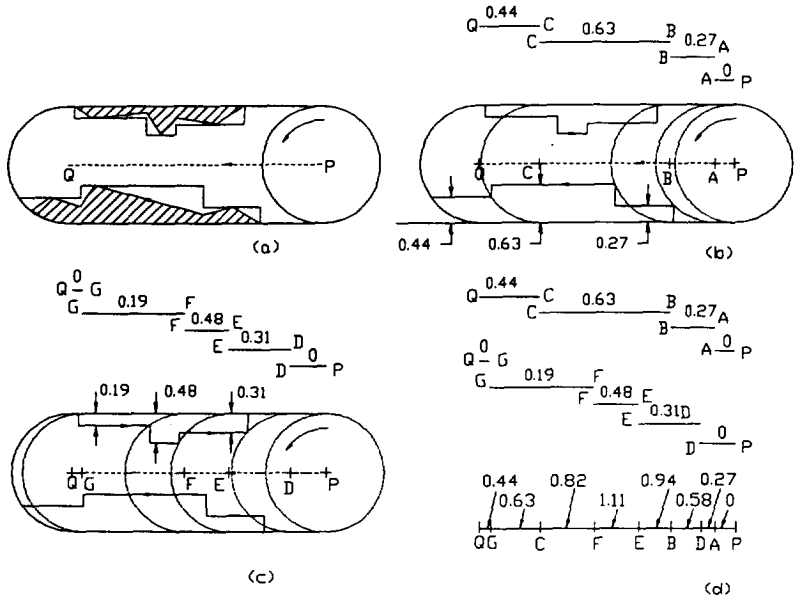

FIG. 9. Radial width of cut in combined up- and down-milling.

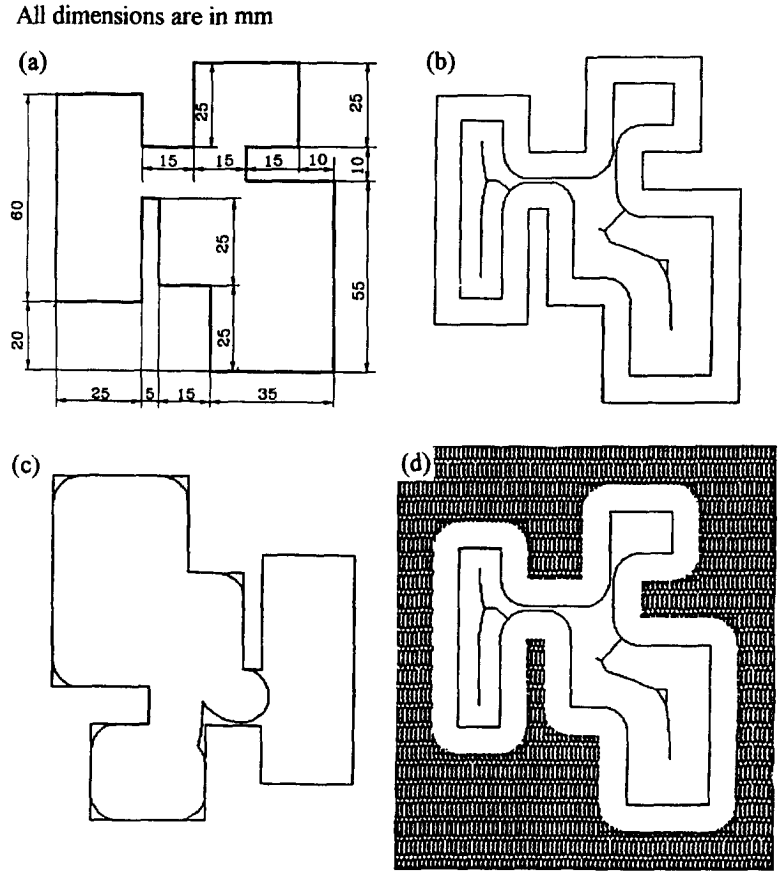

FIG. 10. (a) Dimensions of the pocket; (b) tool path generated (D = 14, b/D = 0.8); (c) machined graph during simulation of cutting; (d) final result after simulation.

segments. The results are summarized in Tables 3(a) and 3(b). The radial width of cut varied from 0 to 14 mm; rather than show the radial width of cut for each of the 130 segments, the total distance travelled by the cutter for a width of cut range is shown. From these tables, it is clear that even though the aim is to minimize slotting, it occurs over 40% of the total distance. Only during 10% of the travel, is the radial width of cut in the range 9.0–9.5 mm and for another 10% in the range 8.0–8.5 mm. These values can be attributed to the relationship between the cutter diameter and the shape of the pocket. For this pocket, whose boundary includes three constrictions, it may be better to use a smaller cutter diameter. Had the shape of the pocket been regular (i.e. rectangular or circular), then a greater proportion of the actual radial widths of cut would have been equal to the assumed value of 9.8 mm.

Note that for nearly 18% of its travel, the radial width of cut is zero. The strategy adopted by the TECHMILL system [10–12] is not to lift the cutter in a finishing operation and this often results in the cutter having to travel over previously machined surfaces. Lifting the cutter may result in a "stepped" surface due to the repositioning inaccuracies in the machine tool. Figure 10(c) shows the machined graph at a particular

TABLE 3. (a) DISTANCES TRAVELLED FOR DIFFERENT RADIAL WIDTHS OF CUT

Radial width of cut (mm)	Total travel (mm)
0	188.344
0–0.5	0.035
0.5–1.0	0.0
1.0–1.5	20.0
1.5–2.0	6.934
2.0–2.5	1.135
2.5–3.0	5.155
3.0–3.5	55.016
3.5–4.0	1.497
4.0–4.5	0.0
4.5–5.0	0.0
5.0–5.5	6.261
5.5–6.0	0.0
6.0–6.5	35.22
6.5–7.0	6.416
7.0–7.5	34.727
7.5–8.0	0.0
8.0–8.5	111.255
8.5–9.0	3.248
9.0–9.5	109.351
9.5–10.0	12.806
10.0–10.5	23.673
10.5–11.0	0.0
11.0–11.5	0.0921
11.5–12.0	3.701
12.0–12.5	4.46
12.5–13.0	15.463
13.0–13.5	8.745
13.5–14.0	401.345

TABLE 3. (b) DISTANCES TRAVELLED WITH DIFFERENT CUTTING MODES

MODE	LENGTH (MM)
SLOTTING	430.013
UP-MILLING	10.202
DOWN-MILLING	453.329
CUTTING AIR	188.344
SYMMETRICAL MILLING	1.659

Total length = 1054.879.

instant during the cutting process and Fig. 10(d) the final simulated result. Since the corners in Fig. 10(a) have been specified as sharp, some material at the corners remains unmachined [see Fig. 10(c)].

8. CONCLUSION

In this paper a direct method to determine the actual width of cut and the cutting mode is presented. It is based on a 2-D Boolean union between the area swept by the cutter and the previously machined area. The actual widths of cut are different from the value assumed to calculate the toolpaths. Instead of using a global value of the radial width of cut to optimize the feedrate and cutting velocity, local values of the radial width of cut can be calculated and used to determine the true optimum values for the feedrate and cutting velocity.

Acknowledgement—The authors wish to thank Ms M. Bancroft for her valuable help in preparing this paper.

REFERENCES

[1] W. A. KLINE, R. E. DEVOR and J. LINDBERG, Prediction of cutting forces in end milling with application to cornering cuts, *Int. J. Mach. Tool Des. Res.* **22**, 7–22 (1982).
[2] W. P. WANG, Solid modelling for optimizing metal removal of three dimensional NC end milling, *J. Manufact. Syst.* **7**(1), (1988).
[3] K. K. WANG, Application of solid modelling to automate machining parameters for complex parts, *Proc. of CIRP Manufacturing Seminar*, Penn State, U.S.A., 33–37 (1987).
[4] M. D. TAKATA, M. INUI TSAI and T. SATA, A cutting simulation system for machinability evaluation using a workpiece model, *Ann. CIRP* **38**(1), 417–420 (1989).
[5] K. D. BOUZAKIS, K. EFSTATHIOU and R. PARASKEVOPOULU, NC-code preparation with optimum cutting conditions in 3-axis milling, *Ann. CIRP* **41**(1), 513–516 (1992).
[6] T. V. HOOK, Real time shaded NC milling display, *Comput. Graphics*, **20**(4), 15–19 (1986).
[7] W. P. WANG and K. K. WANG, Geometric modelling for swept volume of moving solids, *IEEE C G & A*, 57–65 (1986).
[8] W. P. WANG and K. K. WANG, Real-time verification of multi-axis NC programs with raster graphics, *Proc. of IEEE Int. Conf. on Robotics & Automation*, San Francisco, CA, 7–10 April (1986).
[9] M. E. MORTENSON, *Geometric Modelling*. John Wiley, New York (1985).
[10] T. L. LAU, Optimization of milling conditions, Ph.D. thesis, University of Manchester, U.K. (1987).
[11] J. C. E. FERREIRA and S. HINDUJA, Convex hull-based feature recognition method for 2.5D components, *CAD* **22**(1), 41–49 (1990).
[12] R. ENPARANTZA, Tool selection and cutting conditions optimisation in milling, Ph.D. thesis, University of Manchester, U.K. (1991).